Available online at www.sciencedirect.com

ScienceDirect

Ceramics International 40 (2014) 2389–2393

CERAMICS INTERNATIONAL

www.elsevier.com/locate/ceramint

Hydrogenation and dehydrogenation rates of oxide Fe_2O_3-added magnesium, and effects of Ti addition

Myoung Youp Song[a,*], Young Jun Kwak[b], Hye Ryoung Park[c]

[a]Division of Advanced Materials Engineering, Hydrogen & Fuel Cell Research Center, Engineering Research Institute, Chonbuk National University, 567 Baekje-daero Deokjin-gu, Jeonju 561-756, Republic of Korea

[b]Department of Materials Engineering, Graduate School, Chonbuk National University, 567 Baekje-daero Deokjin-gu, Jeonju 561-756, Republic of Korea

[c]Faculty of Applied Chemical Engineering, Chonnam National University, 77 Yongbong-ro Buk-gu, Gwangju 500-757, Republic of Korea

Received 12 July 2013; accepted 2 August 2013
Available online 11 August 2013

Abstract

Samples with compositions of 80 wt% Mg–14 wt% Ni–6 wt% Fe_2O_3, 80 wt% Mg–14 wt% Ni–6 wt% Ti, 80 wt% Mg–14 wt% Ni–3 wt% Fe_2O_3–3 wt% Ti, and 80 wt% Mg–14 wt% Ni–2 wt% Fe_2O_3–2 wt% Ti–2 wt% Fe were prepared by reactive mechanical grinding. Their hydriding and dehydriding properties were then examined and effects of Ti addition on the hydrogen storage properties of Mg–Ni alloys were investigated. The specific surface area of Mg–14Ni–6Fe_2O_3 decreased after activation. On the other hand, the specific surface areas of the samples Mg–14Ni–6Ti, Mg–14Ni–2Fe_2O_3–2Ti–2Fe, and Mg–14Ni–3Fe_2O_3–3Ti, which contain Ti, increased after activation. This proves that the addition of Ti helps the decrease in particle size with hydriding–dehydriding cycling, and prevents the particles from being sintered. Ti forms Ti hydride during reactive mechanical grinding, and remains undecomposed even after dehydriding reaction.

Keywords: Oxide Fe_2O_3; Magnesium; Hydrogenation; Ti addition; Specific surface area

1. Introduction

Hydrogen can be produced from excess alternative energies such as wind, solar, tidal or geothermal energy. When hydrogen is converted into energy by a reaction with oxygen, water is the only exhaust product. So, it does not cause environmental contamination as an energy carrier.

Hydrogen storage by metal hydrides has advantages compared with other hydrogen method such as pressure storage and cryogenic storage. It can store more hydrogen per unit volume, and is safer than other storage methods. It can also use waste heat for release hydrogen from metal hydrides.

Magnesium has many merits as a hydrogen storage material but its reaction rates with hydrogen are very low [1]. A lot of work to improve the hydriding and dehydriding rates of magnesium has been performed by alloying with magnesium certain metals such as Cu [2], Ni [3,4], and In [5], by synthesizing compounds such as $CeMg_{12}$ [6] and $Mg_{76}Ti_{12}Fe_{12-x}Ni_x$ (x=4, 8) [7], and by making composites such as Mg–20 wt% $Fe_{23}Y_8$ [8], Mg–20 wt% Ni–Y [9], Mg–Sn [10], and Mg–V [11]. Aminorroaya et al. [12] added Nb and multi-walled carbon nanotubes to Mg–Ni alloys, and Cho et al. [13] added transition metals to cast Mg–Ni alloys for the improvement of the reaction rates of Mg with H_2. Milanese et al. [14] mixed Ni and Cu with Mg, Tanguy et al. [15] mixed metal additives with magnesium, and Eisenberg et al. [16] plated nickel on the surface of magnesium to improve the hydriding–dehydriding kinetics of MgH_2.

Magnesium is ductile, and thus it is hard to grind magnesium into fine particles. During mechanical grinding the oxides may be pulverized since they are brittle. The added oxides and the pulverized oxides during mechanical grinding can help the particles of magnesium become finer.

The magnesium prepared by mechanical grinding under H_2 (reactive mechanical grinding) with transition elements or oxides showed relatively high hydriding and dehydriding rates when the content of the additives was about 20 wt%.

*Corresponding author. Tel.: +82 63 270 2379; fax: +82 63 270 2386.
E-mail addresses: songmy@jbnu.ac.kr, songmy@chonbuk.ac.kr (M.Y. Song).

0272-8842/$ - see front matter © 2013 Elsevier Ltd and Techna Group S.r.l. All rights reserved.
http://dx.doi.org/10.1016/j.ceramint.2013.08.010

Addition of Fe_2O_3 prepared by spray conversion to Mg with reactive mechanical grinding improved greatly the hydriding rate of Mg [17]. But the preparation of Fe_2O_3 prepared by spray conversion is a complicated process. We thus used purchased Fe_2O_3 to prepare the samples. An addition of too much Fe_2O_3 will decrease the hydrogen storage capacity. We added less than 6 wt% to get a high effect of the oxide addition without decreasing the hydrogen storage capacity severely.

Reilly et al. [3] and Akiba et al. [4] improved the reaction kinetics of Mg with H_2 by preparing Mg–Ni alloys. Song et al. [18–21] increased the hydriding and dehydriding rates of Mg by mechanical alloying of Mg with Ni under Ar atmosphere. Bobet et al. [22] improved the hydrogen-storage properties of both magnesium and Mg+10 wt% Co, Ni, or Fe mixtures by reactive mechanical grinding for a short time (2 h). We chose Ni and Fe as transition elements to be added. Ti was also selected since it was considered to increase the hydriding and dehydriding rates when it was added.

In this work, samples with compositions of 80 wt% Mg–14 wt% Ni–6 wt% Fe_2O_3, 80 wt% Mg–14 wt% Ni–6 wt% Ti, 80 wt% Mg–14 wt% Ni–3 wt% Fe_2O_3–3 wt% Ti, and 80 wt% Mg–14 wt% Ni–2 wt% Fe_2O_3–2 wt% Ti–2 wt% Fe were prepared by reactive mechanical grinding. Their hydriding and dehydriding properties were then examined and effects of Ti addition on the hydrogen storage properties of Mg–Ni alloys were investigated. We designated 80 wt% Mg–14 wt% Ni–6 wt% Fe_2O_3, 80 wt% Mg–14 wt% Ni–6 wt% Ti, 80 wt% Mg–14 wt% Ni–3 wt% Fe_2O_3–3 wt% Ti, and 80 wt% Mg–14 wt% Ni–2 wt% Fe_2O_3–2 wt% Ti–2 wt% Fe as Mg–14Ni–6Fe_2O_3, Mg–14Ni–6Ti, Mg–14Ni–3Fe_2O_3–3Ti, and Mg–14Ni–2Fe_2O_3–2Ti–2Fe, respectively.

2. Experimental details

Pure Mg powder (particle size 297 − 100 μm, purity 99%, Fluka), Ni (average particle size ~5 μm, purity 99.9%, Cerac), Fe_2O_3 (average particle size < 5 μm, purity ≥ 99%, Aldrich), Ti (~44 μm, purity 99.9%, Aldrich), and Fe (spherical, particle size < 10 μm, purity 99.5 %, Alfa Aesar GmbH) were used as starting materials.

Reactive mechanical grinding was done in a planetary ball mill (Planetary Mono Mill; Pulverisette 6, Fritsch). A mixture with the desired composition (total weight = 8 g) was mixed in a stainless steel container (with 105 hardened steel balls, total weight = 360 g) sealed hermetically. The sample to ball weight ratio was 1/45. All sample handling was performed in a glove box under Ar in order to prevent oxidation. The disc revolution speed was 250 rpm. The mill container (volume of 250 ml) was then filled with high purity hydrogen gas (about 12 bar). The reactive mechanical grinding was performed for 6 h (milling 2 h + refilling with H_2 + milling 2 h + refilling with H_2 + milling 2 h).

The absorbed or desorbed hydrogen quantity was measured as a function of time by a volumetric method, using a Sievert's type hydriding and dehydriding apparatus described previously [23]. 0.5 g of the samples was used for the measurement of the absorbed or desorbed hydrogen quantity as a function of time. X-ray diffraction (XRD) analysis was carried out for the as-milled powders and for the samples after hydriding–dehydriding cycling. The microstructures were observed by scanning electron microscopy (SEM).

3. Results and discussion

Fig. 1 shows TGA curves at 373–673 K for Mg–14Ni–6Fe_2O_3, Mg–14Ni–6Ti, Mg–14Ni–3Fe_2O_3–3Ti, and Mg–14Ni–2Fe_2O_3–2Ti–2Fe after reactive mechanical grinding. The curves represent rapid decreases in the temperature range of about 473–583 K. The weight in the curve for Mg–14Ni–6Fe_2O_3 decreases slowly from 373 K, and then decreases rapidly from about 473 K to about 583 K. The weight in the curve for Mg–14Ni–6Ti decreases very slowly from 373 K, and then decreases rapidly from about 473 K to about 513 K. The weight in the curve for Mg–14Ni–3Fe_2O_3–3Ti remains constant from 373 K, and then decreases rapidly from about 473 K to about 543 K. The weight in the curve for Mg–14Ni–2Fe_2O_3–2Ti–2Fe decreases very slowly from 373 K, and then decreases rapidly from about 473 K to about 523 K. Mg–14Ni–6Fe_2O_3, Mg–14Ni–6Ti, Mg–14Ni–3Fe_2O_3–3Ti, and Mg–14Ni–2Fe_2O_3–2Ti–2Fe represent decreases of 6.91, 2.59, 3.34, and 3.24 wt%, respectively, in the temperature

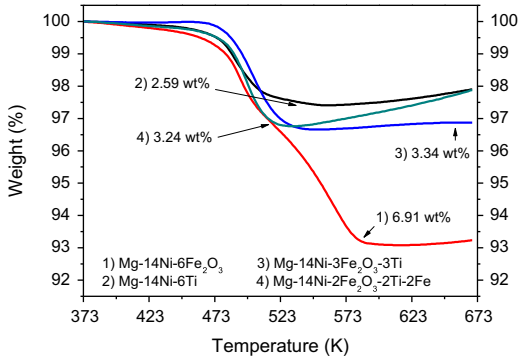

Fig. 1. TGA curves for Mg–14Ni–6Fe_2O_3, Mg–14Ni–6Ti, Mg–14Ni–3Fe_2O_3–3Ti, and Mg–14Ni–2Fe_2O_3–2Ti–2Fe alloys.

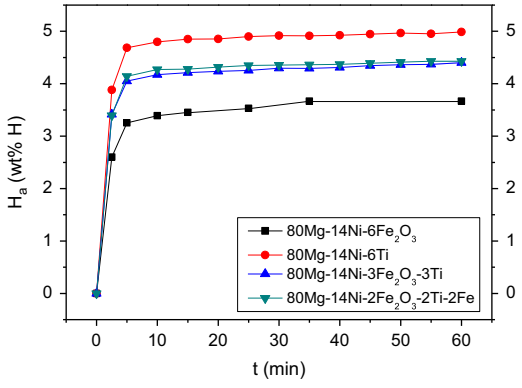

Fig. 2. Variation of H_a vs. t curve with sample; Mg–14Ni–6Fe_2O_3, Mg–14Ni–6Ti, Mg–14Ni–3Fe_2O_3–3Ti, and Mg–14Ni–2Fe_2O_3–2Ti–2Fe at 573 K under 12 bar H_2 after activation (at n = 3).

range of 373–583 K. The increases in the weights of samples after decrease in the sample weights are due to buoyancy effect, a phenomenon that weight seems to increase since the gas density decreases as temperature rises.

The percentage of absorbed hydrogen H_a is expressed with respect to sample weight. The variation of H_a vs. t curve with sample; Mg–14Ni–6Fe_2O_3, Mg–14Ni–6Ti, Mg–14Ni–3Fe_2O_3–3Ti, and Mg–14Ni–2Fe_2O_3–2Ti–2Fe at 573 K under 12 bar H_2 after activation (at $n=3$) is shown in Fig. 2. The curves exhibit very high hidriding rates from the beginning to about 5 min, and then extremely low hidriding rates. Mg–14Ni–6Ti has the highest hydriding rate and the largest value of H_a after 60 min, followed in order by Mg–14Ni–2Fe_2O_3–2Ti–2Fe, Mg–14Ni–3Fe_2O_3–3Ti, and Mg–14Ni–6Fe_2O_3. The H_a values for 5 min of Mg–14Ni–6Ti, Mg–14Ni–2Fe_2O_3–2Ti–2Fe, Mg–14Ni–3Fe_2O_3–3Ti, and Mg–14Ni–6Fe_2O_3 are 4.69, 4.14, 4.05, and 3.25 wt% H, respectively. The H_a values for 60 min of Mg–14Ni–6Ti, Mg–14Ni–2Fe_2O_3–2Ti–2Fe, Mg–14Ni–3Fe_2O_3–3Ti, and Mg–14Ni–6Fe_2O_3 are 4.99, 4.43, 4.40, and 3.67 wt% H, respectively.

The percentage of desorbed hydrogen H_d is also expressed with respect to sample weight. Fig. 3 presents the variation of H_d vs. t curve with sample; Mg–14Ni–6Fe_2O_3, Mg–14Ni–6Ti, Mg–14Ni–3Fe_2O_3–3Ti, and Mg–14Ni–2Fe_2O_3–2Ti–2Fe at 573 K under 1.0 bar H_2 after activation (at $n=3$). The H_d value increases almost linearly with time, and then the dehydriding rate gets very low after 25 min for Mg–14Ni–6Ti, after 20 min for Mg–14Ni–3Fe_2O_3–3Ti, after about 35 min for Mg–14Ni–2Fe_2O_3–2Ti–2Fe, and after about 40 min for Mg–14Ni–6Fe_2O_3. Mg–14Ni–6Ti has the highest dehydriding rate, followed in order by Mg–14Ni–3Fe_2O_3–3Ti, Mg–14Ni–2Fe_2O_3–2Ti–2Fe, and Mg–14Ni–6Fe_2O_3. The H_d values for 20 min of Mg–14Ni–6Ti, Mg–14Ni–3Fe_2O_3–3Ti, Mg–14Ni–2Fe_2O_3–2Ti–2Fe, and Mg–14Ni–6Fe_2O_3 are 4.38, 3.81, 2.06, and 1.61 wt% H, respectively. Mg–14Ni–6Ti has the largest value of H_d after 60 min, followed in order by Mg–14Ni–3Fe_2O_3–3Ti, Mg–14Ni–6Fe_2O_3, and Mg–14Ni–2Fe_2O_3–2Ti–2Fe with their values being 4.98, 4.16, 3.37, and 3.29 wt% H, respectively.

Fig. 4 shows BET graphs [$1/\{V_a(P_o/P-1)\}$ vs. P/P_o plots] for Mg–14Ni–6Fe_2O_3, Mg–14Ni–6Ti, Mg–14Ni–3Fe_2O_3–3Ti, and Mg–14Ni–2Fe_2O_3–2Ti–2Fe after reactive mechanical grinding, where V_a is the volume of adsorbed gas, P_o is the saturated pressure of adsorbed gas, and P is the equilibrium pressure of adsorbed gas. According to BET equation the specific surface area is large when the plot $1/\{V_a(P_o/P-1)\}$ vs. P/P_o has a small slope

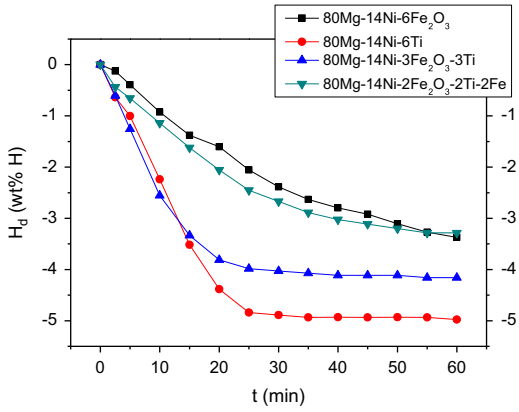

Fig. 3. Variation of H_d vs. t curve with sample; Mg–14Ni–6Fe_2O_3, Mg–14Ni–6Ti, Mg–14Ni–3Fe_2O_3–3Ti, and Mg–14Ni–2Fe_2O_3–2Ti–2Fe at 573 K under 1.0 bar H_2 after activation (at $n=3$).

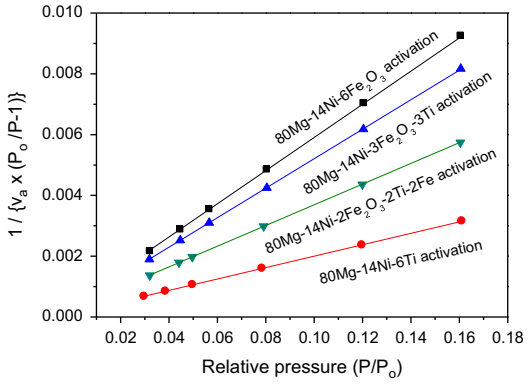

Fig. 5. BET graphs [$1/\{V_a(P_o/P-1)\}$ vs. P/P_o plots] for Mg–14Ni–6Fe_2O_3, Mg–14Ni–6Ti, Mg–14Ni–3Fe_2O_3–3Ti, and Mg–14Ni–2Fe_2O_3–2Ti–2Fe after activation.

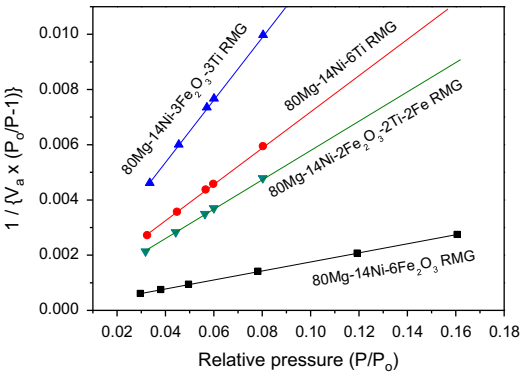

Fig. 4. BET graphs [$1/\{V_a(P_o/P-1)\}$ vs. P/P_o plots] for Mg–14Ni–6Fe_2O_3, Mg–14Ni–6Ti, Mg–14Ni–3Fe_2O_3–3Ti, and Mg–14Ni–2Fe_2O_3–2Ti–2Fe after reactive mechanical grinding.

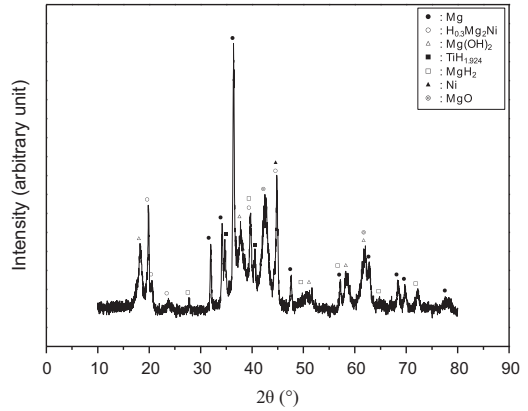

Fig. 6. XRD pattern of Mg–14Ni–6Ti dehydrided at the fourth hydriding–dehydriding cycle.

Table 1
Absorbed and desorbed hydrogen quantity, BET surface area after reactive mechanical grinding and after activation for Mg–14Ni–6Fe_2O_3, Mg–14Ni–6Ti, Mg–14Ni–3Fe_2O_3–3Ti, and Mg–14Ni–2Fe_2O_3–2Ti–2Fe.

	H_a for 60 min at $n=1$ (wt% H)	H_d for 60 min at $n=1$ (wt% H)	H_a for 60 min at $n=3$ (wt% H)	H_d for 60 min at $n=3$ (wt% H)	BET surface area after reactive mechanical grinding (m^2/g)	BET surface area after activation (m^2/g)
Mg–14Ni–6Fe_2O_3	3.02	2.86	3.67	3.37	265	78
Mg–14Ni–6Ti	4.91	4.80	4.99	4.98	64	229
Mg–14Ni–3Fe_2O_3–3Ti	4.29	3.99	4.40	4.16	38	89
Mg–14Ni–2Fe_2O_3–2Ti–2Fe	4.56	3.33	4.43	3.29	79	127

and a small value of intercept on the vertical axis. The plots show that Mg–14Ni–6Fe_2O_3 has the largest specific surface area, followed in order by those of Mg–14Ni–2Fe_2O_3–2Ti–2Fe, Mg–14Ni–6Ti, Mg–14Ni–3Fe_2O_3–3Ti.

BET graphs [$1/\{V_a(P_o/P-1)\}$ vs. P/P_o plots] for Mg–14Ni–6Fe_2O_3, Mg–14Ni–6Ti, Mg–14Ni–3Fe_2O_3–3Ti, and Mg–14Ni–2Fe_2O_3–2Ti–2Fe after activation are presented in Fig. 5. The plots show that Mg–14Ni–6Ti has the largest specific surface area, followed in order by those of Mg–14Ni–2Fe_2O_3–2Ti–2Fe, Mg–14Ni–3Fe_2O_3–3Ti, and Mg–14Ni–6Fe_2O_3.

Fig. 6 shows the XRD pattern of Mg–14Ni–6Ti dehydrided at the fourth hydriding–dehydriding cycle. The sample contains Mg, $H_{0.3}Mg_2Ni$, MgO, $Mg(OH)_2$, MgH_2, Ni, and $TiH_{1.924}$ phases. This shows that Mg_2NiH_4 is formed by the reaction of Mg with Ni and hydrogen during hydriding–dehydriding cycling, and the Mg_2NiH_4 phase becomes the $H_{0.3}Mg_2Ni$ phase after dehydriding reaction. $Mg(OH)_2$ is considered to be formed by the reaction of Mg with water vapor. $TiH_{1.924}$, which was formed during reactive mechanical grinding, remains undecomposed after dehydriding. The XRD patterns of dehydrided Mg–14Ni–2Fe_2O_3–2Ti–2Fe and Mg–14Ni–3Fe_2O_3–3Ti after hydriding–dehydriding cycling revealed Mg, MgH_2, Mg_2Ni, MgO, Fe_2O_3, Fe, and $TiH_{1.924}$ phases.

Table 1 gives the absorbed and desorbed hydrogen quantity, BET surface area after reactive mechanical grinding and after activation for Mg–14Ni–6Fe_2O_3, Mg–14Ni–6Ti, Mg–14Ni–3Fe_2O_3–3Ti, and Mg–14Ni–2Fe_2O_3–2Ti–2Fe. After reactive mechanical grinding, Mg–14Ni–6Fe_2O_3 has the largest specific surface area (265 m^2/g), followed in order by Mg–14Ni–2Fe_2O_3–2Ti–2Fe (79 m^2/g), Mg–14Ni–6Ti (64 m^2/g), and Mg–14Ni–3Fe_2O_3–3Ti (38 m^2/g). After activation, Mg–14Ni–6Ti has the largest specific surface area (229 m^2/g), followed in order by Mg–14Ni–2Fe_2O_3–2Ti–2Fe (127 m^2/g), and Mg–14Ni–3Fe_2O_3–3Ti (89 m^2/g), and Mg–14Ni–6Fe_2O_3 (78 m^2/g).

Fig. 1 shows that Mg–14Ni–6Fe_2O_3 represents decrease of 6.91 wt% in the temperature range of about 373–583 K. This shows that Mg–14Ni–6Fe_2O_3 absorbs 6.91 wt% of hydrogen during reactive mechanical grinding, and the addition of Fe_2O_3 is very effective for increasing the hydriding rate of Mg–Ni alloy. Table 1 shows that Mg–14Ni–6Fe_2O_3 after reactive mechanical grinding has a specific surface area of 265 m^2/g, and Mg–14Ni–6Fe_2O_3 after activation has that of 78 m^2/g. The specific surface area of Mg–14Ni–6Fe_2O_3 decreases after activation. On the other hand, the specific surface areas of the samples Mg–14Ni–6Ti, Mg–14Ni–2Fe_2O_3–2Ti–2Fe, and Mg–14Ni–3Fe_2O_3—3Ti, which contain Ti, increase after activation. This proves that the addition of Ti helps the decrease in particle size with hydriding–dehydriding cycling, and prevents the particles from being sintered. Ti forms Ti hydride during reactive mechanical grinding, and remains undecomposed even after dehydriding reaction.

4. Conclusions

Mg–14Ni–6Fe_2O_3 represented decrease of 6.91 wt% in the temperature range of about 373–583 K, showing that Mg–14Ni–6Fe_2O_3 absorbed 6.91 wt% of hydrogen during reactive mechanical grinding. The specific surface area of Mg–14Ni–6Fe_2O_3 decreased after activation. On the other hand, the specific surface areas of the samples Mg–14Ni–6Ti, Mg–14Ni–2Fe_2O_3–2Ti–2Fe, and Mg–14Ni–3Fe_2O_3–3Ti, which contain Ti, increased after activation. This proves that the addition of Ti helps the decrease in particle size with hydriding–dehydriding cycling, and prevents the particles from being sintered. Ti forms Ti hydride during reactive mechanical grinding, and remains undecomposed even after dehydriding reaction.

Acknowledgement

This work was also supported by the selection of research-oriented professor (Myoung Youp Song) of Chonbuk National University in 2013.

References

[1] A. Vose, Metal Hydrides, U.S. Patent 2,944, 587, 1961.
[2] J.J. Reilly, R.H. Wiswall, Inorganic Chemistry 6 (12) (1967) 2220.
[3] J.J. Reilly, R.H. Wiswall Jr, Inorganic Chemistry 7 (11) (1968) 2254.
[4] E. Akiba, K. Nomura, S. Ono, S. Suda, International Journal of Hydrogen Energy 7 (10) (1982) 787.
[5] M.H. Mintz, Z. Gavra, Z. Hadari, Journal of Inorganic and Nuclear Chemistry 40 (1978) 765.

[6] J.M. Boulet, N. Gerard, Journal of the Less Common Metals 89 (1983) 151.
[7] M. Lucaci, A.R. Biris, R.L. Orban, G.B. Sbarcea, V. Tsakiris, Journal of Alloys and Compounds 488 (1) (2009) 163.
[8] Z. Li, X. Liu, Z. Huang, L. Jiang, S. Wang, Rare Metals 25 (6) (2006) 247 (Suppl. 1).
[9] Z. Li, X. Liu, L. Jiang, S. Wang, International Journal of Hydrogen Energy 32 (12) (2007) 1869.
[10] H.C. Zhong, H. Wang, L.Z. Ouyang, M. Zhu, Journal of Alloys and Compounds 509 (11) (2011) 4268.
[11] P. Pei, X. Song, J. Liu, A. Song, P. Zhang, G. Chen, International Journal of Hydrogen Energy 31 (1) (2012) 984.
[12] S. Aminorroaya, A. Ranjbar, Y.H. Cho, H.K. Liu, A.K. Dahle, International Journal of Hydrogen Energy 36 (1) (2011) 571.
[13] Y.H. Cho, S. Aminorroaya, H.K. Liu, A.K. Dahle, International Journal of Hydrogen Energy 36 (8) (2011) 4984.
[14] C. Milanese, A. Girella, G. Bruni, P. Cofrancesco, V. Berbenni, P. Matteazzi, A. Marini, Intermetallics 18 (2) (2010) 203.
[15] B. Tanguy, J.L. Soubeyroux, M. Pezat, J. Portier, P. Hagenmuller, Materials Research Bulletin 11 (1976) 1441.
[16] F.G. Eisenberg, D.A. Zagnoli, J.J. Sheridan III, Journal of the Less Common Metals 74 (1980) 323.
[17] M.Y. Song, I.H. Kwon, S.N. Kwon, C.G. Park, S.H. Hong, D.R. Mumm, J.S. Bae, Journal of Alloys and Compounds 415 (2006) 266.
[18] M.Y. Song, Journal of Materials Science 30 (1995) 1343.
[19] M.Y. Song, E.I. Ivanov, B. Darriet, M. Pezat, P. Hagenmuller, International Journal of Hydrogen Energy 10 (3) (1985) 169.
[20] M.Y. Song, E.I. Ivanov, B. Darriet, M. Pezat, P. Hagenmuller, Journal of the Less Common Metals 131 (1987) 71.
[21] M.Y. Song, International Journal of Hydrogen Energy 20 (3) (1995) 221.
[22] J.-L. Bobet, E. Akiba, Y. Nakamura, B. Darriet, International Journal of Hydrogen Energy 25 (2000) 987.
[23] S.N. Kwon, Improvement of hydriding and dehydriding rates of Mg-based hydrogen storage alloys due to catalytic effects of Fe_2O_3 and Ni, (Thesis of Master of Engineering), Chonbuk National University, Jeonju, South Korea, 2007.